

CONSTRAINTS ON LONG-PERIOD PLANETS FROM AN L' - AND M -BAND SURVEY OF NEARBY SUN-LIKE STARS: MODELING RESULTS*

A. N. HEINZE¹, PHILIP M. HINZ¹, MATTHEW KENWORTHY¹, MICHAEL MEYER², SURESH SIVANANDAM¹, AND DOUGLAS MILLER¹

¹ Steward Observatory, University of Arizona, 933 N. Cherry Avenue, Tucson, AZ 85721, USA; ariheinze@hotmail.com, phinz@as.arizona.edu, mkenworthy@as.arizona.edu, suresh@as.arizona.edu, dlmiller@as.arizona.edu

² Department of Physics, Swiss Federal Institute of Technology (ETH-Zurich), ETH Hönggerberg, CH-8093 Zurich, Switzerland; mmeyer@phys.ethz.ch

Received 2009 August 28; accepted 2010 March 2; published 2010 April 21

ABSTRACT

We have carried out an L' - and M -band adaptive optics (AO) extrasolar planet imaging survey of 54 nearby, Sun-like stars using the Clio camera at the MMT. Our survey concentrates more strongly than all others to date on very nearby F, G, and K stars, in that we have prioritized proximity higher than youth. Our survey is also the first to include extensive observations in the M band, which supplemented the primary L' observations. These longer-wavelength bands are most useful for very nearby systems in which low-temperature planets with red IR colors (i.e., $H - L'$, $H - M$) could be detected. The survey detected no planets, but set interesting limits on planets and brown dwarfs in the star systems we investigated. We have interpreted our null result by means of extensive Monte Carlo simulations and constrained the distributions of extrasolar planets in mass M and semimajor axis a . If planets are distributed according to a power law with $dN \propto M^\alpha a^\beta dM da$, normalized to be consistent with radial velocity (RV) statistics, we find that a distribution with $\alpha = -1.1$ and $\beta = -0.46$, truncated at 110 AU, is ruled out at the 90% confidence level. These particular values of α and β are significant because they represent the most planet-rich case consistent with current statistics from RV observations. With 90% confidence no more than 8.1% of stars like those in our survey have systems with three widely spaced, massive planets like the A star HR 8799. Our observations show that giant planets in long-period orbits around Sun-like stars are rare, confirming the results of shorter-wavelength surveys and increasing the robustness of the conclusion.

Key words: astrometry – infrared: planetary systems – instrumentation: adaptive optics – planetary systems – planets and satellites: detection

1. INTRODUCTION

Nearly 400 extrasolar planets have now been discovered using the radial velocity (RV) method. RV surveys currently have good statistical completeness only for planets with periods of less than 10 years (Cumming et al. 2008; Butler et al. 2006; Fischer & Valenti 2005) due to the limited temporal baseline of the observations, and the need to observe for a complete orbital period to confirm the properties of a planet with confidence. The masses of discovered planets range from just a few Earth masses (Bouchy et al. 2009) up to around 20 Jupiter masses (M_{Jup}). We note that a $20 M_{\text{Jup}}$ object would be considered by many to be a brown dwarf rather than a planet, but that there is no broad consensus on how to define the upper mass limit for planets. For a good overview of RV planets to date, see Butler et al. (2006) or <http://exoplanet.eu/catalog-RV.php>.

The large number of RV planets makes it possible to examine the statistics of extrasolar planet populations. Several groups have fit approximate power-law distributions in mass and semimajor axis to the set of known extrasolar planets (see, for example, Cumming et al. 2008). Necessarily, however, these power laws are not subject to observational constraints at orbital periods longer than 10 years—and it is at these orbital periods that we find giant planets in our own solar system. We cannot obtain a good understanding of planets in general without information on long-period extrasolar planets. Nor can we see how our own solar system fits into the big picture of planet formation in the galaxy without a good census of planets in Jupiter- and Saturn-like orbits around other stars.

Repeatable detections of extrasolar planets (as opposed to one-time microlensing detections) have so far been made by transit detection (e.g., Charbonneau et al. 2000), by RV variations (Mayor & Queloz 1995), by astrometric wobble (Benedict et al. 2006), or by direct imaging (Marois et al. 2008). Of these methods, transits are efficient only for detecting close-in planets. As noted above, precision RV observations have not been going on long enough to detect more than a few planets with periods longer than 10 years, but even as RV temporal baselines increase, long-period planets will remain harder to detect due to their slow orbital velocities. The amplitude of a star's astrometric wobble increases with the radius of its planet's orbit, but decades-long observing programs are still needed to find long-period planets. Direct imaging is the only method that allows us to characterize long-period extrasolar planets on a timescale of months rather than years or decades.

Direct imaging of extrasolar planets is technologically possible at present only in the infrared, based on the planets' own thermal luminosity, not on reflected starlight. The enabling technology is adaptive optics (AO), which allows 6–10 m ground-based telescopes to obtain diffraction-limited IR images several times sharper than those from the *Hubble Space Telescope* (*HST*), despite Earth's turbulent atmosphere. Theoretical models of giant planets indicate that such telescopes should be capable of detecting self-luminous giant planets in large orbits around young, nearby stars. The stars should be young because the glow of giant planets comes from gravitational potential energy converted to heat in their formation and subsequent contraction: lacking any internal fusion, they cool and become fainter as they age.

Several groups have published the results of AO imaging surveys for extrasolar planets around F, G, K, or M stars in

* Observations reported here were obtained at the MMT Observatory, a joint facility of the University of Arizona and the Smithsonian Institution.

the last five years (see, for example, Masciadri et al. 2005; Kasper et al. 2007; Biller et al. 2007; Lafrenière et al. 2007; and Chauvin et al. 2010). Of these, most have used wavelengths in the 1.5–2.2 μm range, corresponding to the astronomical H and K_S filters (Masciadri et al. 2005; Biller et al. 2007; Lafrenière et al. 2007; Chauvin et al. 2010). They have targeted mainly very young stars. Because young stars are rare, the median distance to stars in each of these surveys has been more than 20 pc.

In contrast to those above, our survey concentrates on very nearby F, G, and K stars, with proximity prioritized more than youth in the sample selection. The median distance to our survey targets is only 11.2 pc. Ours is also the first survey to include extensive observations in the M band, and only the second to search solar-type stars in the L' band (the first was Kasper et al. 2007). The distinctive focus on older, very nearby stars for a survey using longer wavelengths is natural: longer wavelengths are optimal for lower-temperature planets which are most likely to be found in older systems, but which would be undetectable around all but the nearest stars. More information on our sample selection, observations, and data analysis can be found in our observations paper, Heinze et al. (2010), which also details our careful evaluation of our survey's sensitivity, including extensive tests in which fake planets were randomly placed in the raw data and then recovered by an experimenter who knew neither their positions nor their number. Such tests are essential for establishing the true relationship between source significance (i.e., 5σ , 10σ , etc.) and survey completeness.

Our survey places constraints on a more mature population of planets than those that have focused on very young stars, and confirms that a paucity of giant planets at large separations from Sun-like stars is robustly observed at a wide range of wavelengths.

In Section 2, we review power-law fits to the distribution of known RV planets, including the normalization of the power laws. In Section 3, we present the constraints our survey places on the distribution of extrasolar giant planets, based on extensive Monte Carlo simulations. In Section 4, we discuss the promising future of planet-search observations in the L' and especially the M band, and in Section 5 we conclude.

2. STATISTICAL DISTRIBUTIONS FROM RV PLANETS

Nearly 400 RV planets are known; see Butler et al. (2006) for a useful, conservative listing of confirmed extrasolar planets as of 2006, or <http://exoplanet.eu/catalog-RV.php> for a frequently updated catalog of all confirmed and many suspected extrasolar planet discoveries.

The number of RV planets is sufficient for meaningful statistical analysis of how extrasolar planets are distributed in terms of their masses and orbital semimajor axes. The lowest-mass planets and those with the longest orbital periods are generally rejected from such analyses to reduce bias from completeness effects, but there remains a considerable range (2–2000 days in period or roughly 0.03–3.1 AU in semimajor axis for solar-type stars; and 0.3–20 M_{Jup} in mass) where RV searches have good completeness (Cumming et al. 2008). There is evidence that the shortest-period planets, or “hot Jupiters,” represent a separate population, a “pileup” of planets in very close-in orbits that does not follow the same statistical distribution as planets in more distant orbits (Cumming et al. 2008). The hot Jupiters are therefore often excluded from statistical fits to the overall populations of extrasolar planets, or at least from the fits to the semimajor axis distribution.

Cumming et al. (2008) characterize the distribution of RV planets detected in the Keck Planet Search with an equation of the form

$$dN = C_0 M^{\alpha_L} P^{\beta_L} d \ln(M) d \ln(P), \quad (1)$$

where M is the mass of the planet, P is the orbital period, and C_0 is a normalization constant. They state that 10.5% of solar-type stars have a planet with mass between 0.3 and 10 M_{Jup} and period between 2 and 2000 days, which can be used to derive a value for C_0 given values for the power-law exponents α_L and β_L . They find that the best-fit values for these are $\alpha_L = -0.31 \pm 0.2$ and $\beta_L = 0.26 \pm 0.1$, where the $_L$ subscript is our notation to make clear that these are the exponents for the form using logarithmic differentials.

In common with a number of other groups, we choose to represent the power law with ordinary differentials, and to give it in terms of orbital semimajor axis a rather than orbital period P :

$$dN = C_0 M^\alpha a^\beta dM da, \quad (2)$$

where C_0 , of course, will not generally have the same value for Equations (1) and (2). Manipulating the two equations and using Kepler's third law make it clear that

$$\alpha = \alpha_L - 1 \quad (3)$$

and

$$\beta = \frac{3}{2} \beta_L - 1. \quad (4)$$

The Cumming et al. (2008) exponents produce $\alpha = -1.31 \pm 0.2$ and $\beta = -0.61 \pm 0.15$ when translated into our form. The mass power law is well behaved, but the integral of the semimajor axis power law does not converge as $a \rightarrow \infty$, so an outer truncation radius is an important parameter of the semimajor axis distribution.

Butler et al. (2006) present the 2006 Catalog of Nearby Exoplanets, a carefully described heterogeneous sample of planets detected by several different RV search programs. With appropriate caution, Butler et al. (2006) refrain from quoting confident power-law slopes based on the combined discoveries of many different surveys with different detection limits and completeness biases (in contrast, the Cumming et al. 2008 analysis was restricted to stars in the Keck Planet Search, which were uniformly observed up to a given minimum baseline and velocity precision). Butler et al. (2006) do tentatively adopt a power law with the form of Equation (2) for mass only and state that α appears to be about -1.1 (or -1.16 , to give the exact result of a formal fit to their list of exoplanets). However, they caution that due to their heterogeneous list of planets discovered by different surveys, this power law should be taken more as a descriptor of the known planets than of the underlying distribution. They do not quote a value for the semimajor axis power-law slope β .

Based mostly on Cumming et al. (2008), but considering Butler et al. (2006) as helpful additional input, we conclude that the true value of the mass power-law slope α is probably between -1.1 and -1.51 , with -1.31 as a good working model. The value of the semimajor axis power-law slope β is probably between -0.46 and -0.76 , with -0.61 as a current best guess. The outer truncation radius of the semimajor axis distribution cannot be constrained by the RV results: surveys like ours exist, in part, to constrain this interesting number.

The only other result we need from the RV searches is a normalization that will allow us to find C_0 . We elect not to use the Cumming et al. (2008) value (10.5% of stars having a

Table 1
L'-band Absolute Magnitudes from Burrows et al. (2003)

Planet Mass (M_{Jup})	Magnitude at 0.10 Gyr	Magnitude at 0.32 Gyr	Magnitude at 1.0 Gyr	Magnitude at 3.2 Gyr	Magnitude at 5.0 Gyr
1.0	19.074	23.010	27.870	33.50 ^a	35.50 ^a
2.0	16.793	19.351	23.737	28.398	29.479
5.0	14.500	16.397	18.588	22.437	24.407
7.0	13.727	15.390	17.336	20.131	21.574
10.0	12.888	14.437	16.246	18.480	19.466
15.0	12.00 ^b	13.61 ^b	14.773	16.816	17.691
20.0	11.30 ^b	12.98 ^b	14.190	15.967	16.766

Notes.

^a No models for these very faint planets appear in Burrows et al. (2003). We have inserted ad hoc values to smooth the interpolations. Any effect of the interpolated magnitudes for planets we could actually detect is negligible.

^b No models for these bright, hot planets appear in Burrows et al. (2003), which focuses on cooler objects. We have added values from Baraffe et al. (2003) and then adjusted them to slightly fainter values to ensure smooth interpolations.

Table 2
M-band Absolute Magnitudes from Burrows et al. (2003)

Planet Mass (M_{Jup})	Magnitude at 0.10 Gyr	Magnitude at 0.32 Gyr	Magnitude at 1.0 Gyr	Magnitude at 3.2 Gyr	Magnitude at 5.0 Gyr
1.0	14.974	16.995	19.987	25.0 ^a	26.0 ^a
2.0	14.023	15.313	17.807	21.295	22.163
5.0	13.014	14.017	15.153	17.167	18.537
7.0	12.618	13.561	14.558	16.126	16.909
10.0	12.189	13.096	14.093	15.315	15.951
15.0	11.55 ^b	12.60 ^b	13.370	14.512	14.990
20.0	11.29 ^b	12.21 ^b	13.069	14.122	14.580

Notes.

^a No models for these very faint planets appear in Burrows et al. (2003). We have inserted ad hoc values to smooth the interpolations. Any effect of the interpolated magnitudes for planets we could actually detect is negligible.

^b No models for these bright, hot planets appear in Burrows et al. (2003), which focuses on cooler objects. We have added values from Baraffe et al. (2003) and then adjusted them to slightly fainter values to ensure smooth interpolations.

planet with mass between 0.3 and 10 M_{Jup} and period between 2 and 2000 days), because this range includes the hot Jupiters, a separate population.

We take our normalization instead from the Carnegie Planet Sample, as described in Fischer & Valenti (2005). Their Table 1 (online only) lists 850 stars that have been thoroughly investigated with RV. They state that all planets with mass at least 1 M_{Jup} and orbital period less than four years have been detected around these stars. Forty-seven of these stars are marked in their Table 1 as having RV planets. Table 2 from Fischer & Valenti (2005) gives the measured properties of 124 RV planets, including those orbiting 45 of the 47 stars listed as planet-bearing in their Table 1. The stars left out are HD 18445 and HD 225261. We cannot find any record of these stars having planets, and therefore as far as we can tell they are typos.

Since all planets with masses above 1 M_{Jup} and periods less than four years orbiting stars in the Fischer & Valenti (2005) list of 850 may be relied upon to have been discovered, we may pick any sub-intervals in this range of mass and period and divide the number of planets falling into these intervals by 850 to obtain our normalization. We selected the range 1–13 M_{Jup} in mass and 0.3–2.5 AU in semimajor axis. Twenty-eight stars, or 3.29% of the 850 in the Fischer & Valenti (2005) list, have one or more planets in this range. Our inner limit of 0.3 AU excludes the hot Jupiters, and thus the 3.29% value provides our final normalization. We note that if we adopt the Cumming et al. (2008) best-fit power laws and use the 3.29% normalization to predict the percentage of stars having planets with masses

between 0.3 and 10 M_{Jup} and orbital periods between 2 and 2000 days, we find a value of 9.3%, which is close to the Cumming et al. (2008) value of 10.5%. The slight difference is probably not significant, but might be viewed as upward bias in the Cumming et al. (2008) value due to the inclusion of the hot Jupiters. In any case, we would not have obtained very different constraints if we had used the Cumming et al. (2008) normalization in our Monte Carlo simulations.

For comparison, among the other papers reporting Monte Carlo simulations similar to ours, Kasper et al. (2007) used a normalization of 3% for planets with semimajor axes of 1–3 AU and masses greater than 1 M_{Jup} . This is close to our value of 3.29% for a similar range. Lafrenière et al. (2007) and Nielsen et al. (2008) fixed α and β in their simulations and let the normalization be a free parameter. Chauvin et al. (2010) obtained their normalization from Cumming et al. (2008), and Nielsen & Close (2009) obtained theirs from Fischer & Valenti (2005).

Juric & Tremaine (2008) provide a helpful mathematical description of the eccentricity distribution of known RV planets:

$$P(\epsilon) = \epsilon e^{-\epsilon^2/(2\sigma^2)}. \quad (5)$$

where $P(\epsilon)$ is the probability of a given extrasolar planet having orbital eccentricity ϵ , e is the root of the natural logarithm, and $\sigma = 0.3$. We find that this mathematical form provides an excellent fit to the distribution of real exoplanet eccentricities from Table 2 of Fischer & Valenti (2005), so we have used it

as our probability distribution to generate random eccentricities for the Monte Carlo simulations we describe in Section 3.

3. CONSTRAINTS ON THE DISTRIBUTION OF PLANETS

3.1. Theoretical Spectra

Burrows et al. (2003) present high-resolution, flux-calibrated theoretical spectra of giant planets or brown dwarfs for ages ranging from 0.1 to 5.0 Gyr and masses from 1 to 20 M_{Jup} (these are available for download from <http://www.astro.princeton.edu/~burrows/>). We have integrated these spectra to give absolute magnitudes in the L' and M filters used in Clio (see Tables 1 and 2), and have found that the results can be reasonably interpolated to give the L' - or M -band magnitudes for all planets of interest for our survey. Baraffe et al. (2003) also present models of giant planets and brown dwarfs, pre-integrated into magnitudes in the popular infrared bands. These models predict slightly better sensitivity to low-mass planets in the L' band and slightly poorer sensitivity in the M band, relative to the Burrows et al. (2003) models. We cannot say if the difference is due to the slightly different filter sets used (MKO for Clio versus Johnson-Glass and Johnson for Baraffe et al. 2003), or if it is intrinsic to the different model spectra used in Burrows et al. (2003) and Baraffe et al. (2003). We have chosen to use the Burrows et al. (2003) models exclusively herein, to avoid any errors due to the slight filter differences. Since the Burrows et al. (2003) models predict poorer sensitivity in the L' band, in which the majority of our survey was conducted, our decision to use them is conservative.

3.2. Introducing the Monte Carlo Simulations

In common with several other surveys (Kasper et al. 2007; Biller et al. 2007; Lafrenière et al. 2007; Chauvin et al. 2010), we have used our survey null result to set upper limits on planet populations via Monte Carlo simulations. In these simulations, we input our sensitivity data in the form of tabular files giving the sensitivity in apparent magnitudes as a function of separation in arcseconds for each star. Various features of our images could cause the sensitivity at a given separation to vary somewhat with position angle: to quantify this, our tabular files give 10 different values at each separation, corresponding to 10 different percentiles ranging from the worst to the best sensitivity attained at that separation. These files are described in detail in Heinze et al. (2010) and are available for download from <http://www.hopewriter.com/Astronomyfiles/Data/SurveyPaper/>.

The Monte Carlo simulations described below allow us to use the observed sensitivity to planets in our survey to calculate directly the probability of a given parameter or set of parameters describing the exoplanet population. This, in turn, allows us to constrain these parameters at a given confidence level. This is a maximum likelihood technique that allows us to incorporate all the individual probability functions of the data, as well as parameterized models of the exoplanet population. The approach is similar to a Bayesian approach. However, we also use the results of the simulations to set confidence limits to the parameters, a more classical approach.

Each Monte Carlo simulation runs with given planet distribution power-law slopes α and β , and a given outer truncation value R_{trunc} for the semimajor axis distribution. Using the normalization described in Section 2, the probability P_{plan} of any given star having a planet between 1 and 20 M_{Jup} is then calculated from the input α , β , and R_{trunc} . In each realization of

our survey, each star is randomly assigned a number of planets, based on Poisson statistics with mean P_{plan} . In most cases, $P_{\text{plan}} \ll 1$, so the most likely number of planets is zero. If the star turns out to have one or more planets, the mass and semimajor axis of each are randomly selected from the input power-law distributions. The eccentricity is randomly selected from the Juric & Tremaine (2008) distribution, and an inclination is randomly selected from the distribution $P(i) \propto \sin(i)$. If the star is a binary, the planet may be dropped from the simulation at this point if the orbit seems likely to be unstable. In general, we consider circumstellar planets to be stable as long as their apastron distance is less than 1/3 the projected distance to the companion star, and circumbinary planets to be stable as long as their periastron distance is at least three times greater than the projected separation of the binary. For planets orbiting low-mass secondaries, a smaller limit on the apastron distance is sometimes imposed, while often circumbinary planets required such distant orbits that they were simply not considered; the details are given in Table 4. For each planet passing the orbital stability checkpoint, a full orbit is calculated using a binary star code written by one of us (M.K.). The projected separation in arcseconds is found, and the magnitude of the planet is calculated from its mass, distance, and age using the Burrows et al. (2003) models.

Two further random choices complete the determination of whether the simulated planet is detected. First, one of the 10 percentiles given in the sensitivity files is randomly selected. Combined with the separation in arcseconds, this selection specifies the sensitivity of our observation at the location of the simulated planet. The second random choice is needed because planets appearing at low significance in our images would have a less than 100% chance of being confidently detected. Our blind sensitivity tests using fake planets placed in our raw data showed that we could confirm 97% of 10σ sources, 46% of 7σ sources, and 16% of 5σ sources, where σ is a measure of the point-spread function (PSF) scale noise in a given region of the image (see Heinze et al. 2010 for details). This second and final random choice in our Monte Carlo simulations is therefore arranged to ensure that a randomly selected 16% of planets with $5\text{--}7\sigma$ significance, and 46% of planets with $7\text{--}10\sigma$ significance, are recorded in the simulation as detected objects. Although we have 97% completeness at 10σ , we choose to consider 100% of simulated planets with 10σ or greater significance to be detected, because at only slightly above 10σ the true completeness certainly becomes 100% for all practical purposes. Note that we have conservatively allowed the detection probabilities to increase stepwise, rather than in a continuous curve, from 5 to 10σ : that is, in our Monte Carlo simulations, planets with $5\text{--}7\sigma$ significance are detected at the 5σ rate from our blind sensitivity tests, while those with $7\text{--}10\sigma$ significance are detected at the 7σ rate.

The low completeness (16%) at 5σ , as determined from our blind sensitivity tests using fake planets, may seem surprising. In these tests, we distinguished between planets that were suggested by a concentration of unusually bright pixels (“noticed”) or else confidently identified as real sources (“confirmed”). Many more planets were noticed than were confirmed: for noticed planets, the rates are 100% at 10σ , 86% at 7σ , and 56% at 5σ . However, very many false positives were also noticed, so sources that are merely noticed but not confirmed do not represent usable detections. The completeness levels we used in our Monte Carlo simulations (16% at 5σ and 46% at 7σ) refer to confirmed sources. No false positives were confirmed in any of

our blind tests. Follow-up observations of suspected sources are costly in terms of telescope time, so a detection strategy with a low false-positive rate is important.

Though sensitivity estimators (and therefore the exact meaning of 5σ) differ among planet imaging surveys, ours was quite conservative, as is explained in Heinze et al. (2010). The low completeness we find at 5σ , which has often been taken as a high-completeness sensitivity limit, should serve as a warning to future workers in this field, and an encouragement to establish a definitive significance–completeness relation through blind sensitivity tests as we have done.

Note that our blind sensitivity tests, covered in Heinze et al. (2010), are completely distinct from the Monte Carlo simulations covered herein. The blind tests involved inserting a little over a hundred fake planets into our raw image data to establish our point-source sensitivity. In our Monte Carlo work, we simulated the orbits, masses, and brightnesses of millions of planets, and compared them to our previously established sensitivity limits to see which planets our survey could have detected.

3.3. A Detailed Look at a Monte Carlo Simulation

To evaluate the significance of our survey and provide some guidance for future work, we have analyzed in detail a single Monte Carlo simulation. We chose the Cumming et al. (2008) best-fit values of $\alpha = -1.31$ and $\beta = -0.61$, with the semimajor axis truncation radius set to 100 AU. Planets could range in mass from 1 to $20 M_{\text{Jup}}$. As described in Section 2, we normalized the planet distributions so that each star had a 3.29% probability of having a planet with semimajor axis between 0.3 and 2.5 AU and mass between 1 and $13 M_{\text{Jup}}$. The simulation consisted of 50,000 realizations of our survey with these parameters. In all, 505,884 planets were simulated, of which 51,879 were detected.

In 38% of the 50,000 realizations, our survey found zero planets, while 37% of the time it found one and 25% of the time it found two or more. The planet distribution we considered in this simulation cannot be ruled out by our survey, since a null result such as we actually obtained turns out not to be very improbable.

The large number of survey realizations in our simulation allows the calculation of precise statistics for potentially detectable planets. The median mass of detected planets in our simulation was $11.36 M_{\text{Jup}}$, the median semimajor axis was 43.5 AU, the median angular separation was 2.86 arcsec, and the median significance was 21.4σ . This last number is interesting because it suggests that, for our survey, any real planet detected was likely to appear at high significance, obvious even on a preliminary, “quick-look” reduction of the data. This suggests that performing such reductions at the telescope should be a high priority, to allow immediate confirmation and follow up if a candidate is seen. Figure 1 presents as a histogram the significance of all planets detected in this Monte Carlo simulation.

We suspected that there would be a detection bias toward very eccentric planets, because these would spend most of their orbits near apastron, where they would be easier to detect. This bias did not appear at any measurable level in our simulation. However, there was a weak but clear bias toward planets in low-inclination orbits, which, of course, spend more of their time at large separations from their stars than do planets with nearly edge-on orbits.

A concern with any planet imaging survey is how strongly the results hinge on the best (i.e., nearest and youngest) few stars.

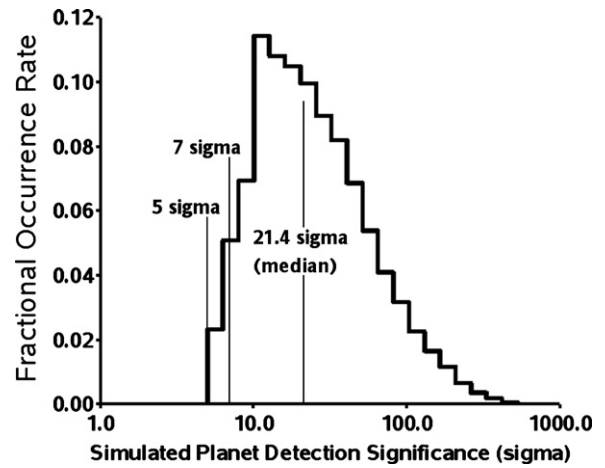


Figure 1. Histogram of detection significance for the 51,879 simulated planets detected in 50,000 realizations of our survey with the Cumming et al. (2008) distribution ($\alpha = -1.31$, $\beta = -0.61$) truncated at 100 AU. Our detection rates went down for significance less than 10σ , but some 5–7 σ planets are still detected. The relatively high median significance of 21.4σ suggests any detected planet would most likely be quite obvious—a good argument for doing “quick-look” data reductions as soon as possible at the telescope.

A survey of 54 stars may have far less statistical power than the number would imply if the best two or three stars had most of the probability of hosting detectable planets. Table 3 gives the percentage of planets detected around each star in our sample based on our detailed Monte Carlo simulation. Due to poor data quality, binary orbit constraints, or other issues, a few stars had zero probability of detected planets given the distribution used here. In general, however, the likelihood of hosting detectable planets is fairly well distributed.

In Table 4, we give the details of planetary orbital constraints used in our Monte Carlo simulations for each binary star we observed, complete with the separations we measured for the binaries. Note that HD 96064 B is a close binary star in its own right, so planets orbiting it were limited in two ways: the apastron could not be too far out or the orbit would be rendered unstable by proximity to HD 96064 A—but the periastron also could not be too far in, or the binary orbit of HD 96064 Ba and HD 96064 Bb would render it unstable. Planets individually orbiting HD 96064 Ba or HD 96064 Bb were not considered in our survey, since to be stable the planets would have to be far too close in for us to detect them. The constraints described in Table 4 account for most of the stars in Table 3 with few or no detections reported.

A final question our detailed simulation can address is how important the M -band observations were to the survey results. In Table 5, we show that when M -band observations were made, they did substantially increase the number of simulated planets detected.

3.4. Monte Carlo Simulations: Constraining the Power Laws

The planet distribution we used in the single Monte Carlo simulation described above could not be ruled out by our survey. To find out what distributions could be ruled out, we performed Monte Carlo simulations assuming a large number of different possible distributions, parameterized by the two power-law slopes α and β , and by the outer semimajor axis truncation radius R_{trunc} . Regardless of the values of α and β , each simulation was normalized to match the RV statistics of Fischer & Valenti (2005): any given star had 3.29% probability of hosting a planet with mass between 1 and $13 M_{\text{Jup}}$ and

Table 3
Percentage of Detected Planets Found Around Each Star

Star Name	Percentage of Total Detected Planets	Median Mass (M_{Jup})	Median Semimajor Axis (AU)	Median Separation (arcsec)
GJ 117	6.07	7.66	39.36	3.64
ϵ Eri	5.83	6.98	18.26	4.35
HD 29391	5.80	8.14	49.13	2.71
GJ 519	4.74	10.44	40.51	3.28
GJ 625	4.67	9.72	29.18	3.48
GJ 5	4.45	9.60	53.42	3.08
BD+60 1417	3.95	11.58	44.48	2.05
GJ 355	3.81	9.71	53.91	2.34
GJ 354.1 A	3.67	9.58	60.12	2.64
GJ 159	3.57	9.73	57.95	2.71
GJ 349	3.35	11.38	44.40	3.17
61 Cyg B	3.29	11.32	19.53	4.08
GJ 879	3.03	11.18	36.84	3.69
GJ 564	2.94	10.67	56.80	2.70
GJ 410	2.93	12.78	41.83	3.03
GJ 450	2.89	12.90	38.72	3.66
GJ 3860	2.68	12.70	49.72	2.69
HD 78141	2.58	12.47	57.00	2.24
BD+20 1790	2.51	12.14	58.33	2.02
GJ 278 C	2.20	12.68	54.56	3.04
GJ 311	2.19	12.55	52.07	3.20
HD 113449	2.17	12.52	59.31	2.29
GJ 211	2.10	13.59	50.51	3.30
BD+48 3686	2.08	12.56	55.05	2.01
GJ 282 A	2.05	13.39	49.85	2.99
GJ 216 A	2.03	12.71	42.98	4.21
61 Cyg A	1.97	13.70	20.94	4.54
HD 1405	1.54	13.13	66.34	2.04
HD 220140 A	1.54	11.73	36.85	1.73
HD 96064 A	1.49	12.63	46.64	1.75
HD 139813	1.43	14.33	59.71	2.37
GJ 380	0.92	15.76	25.31	4.21
GJ 896 A	0.61	12.43	6.47	0.98
GJ 860 A	0.38	11.58	53.26	6.62
τ Ceti	0.38	17.19	25.49	5.52
GJ 896 B	0.34	11.40	6.78	1.14
ξ Boo B	0.32	12.07	8.25	1.36
HD 220140 B	0.28	12.04	25.92	1.37
ξ Boo A	0.24	12.89	8.72	1.50
GJ 659 B	0.21	17.71	62.54	2.81
GJ 166 B	0.17	16.12	6.19	1.34
GJ 684 A	0.17	14.93	85.98	4.87
HD 96064 B	0.13	14.43	38.55	1.60
GJ 505 B	0.12	15.94	17.11	1.61
GJ 166 C	0.10	15.56	6.43	1.52
GJ 505 A	0.07	16.32	18.08	1.75
GJ 702 A	0.02	15.90	6.21	1.50
GJ 684 B	None	NA	NA	NA
GJ 860 B	None	NA	NA	NA
GJ 702 B	None	NA	NA	NA
HD 77407 A	None	NA	NA	NA
GJ 659 A	None	NA	NA	NA
GJ 3876	None	NA	NA	NA
HD 77407 B	None	NA	NA	NA

Notes. This table applies to our detailed Monte Carlo simulation with 50,000 survey realizations run using $\alpha = -1.31$, $\beta = -0.61$, and semimajor axis truncation radius 100 AU. Of all the simulated planets that were detected, we present here the percentage that were found around each given star, and the median mass, semimajor axis, and projected separation for simulated planets found around each star. The table thus indicates around which stars our survey had the highest likelihood of detecting a planet. Many stars with poor likelihood are binaries, with few stable planetary orbits possible.

Table 4
Constraints on Simulated Planet Orbits Around Binary Stars

Star Name	Separation (arcsec)	Constraints on	Constraints on	Constraints on
		Circumprimary Apastron (arcsec, AU)	Circumsecondary Apastron (arcsec, AU)	Circumbinary Periastron (arcsec, AU)
HD 220140 AB	10.828	<3.61, 71.3	<2.17, 42.8	No stable orbits
HD 96064 AB	11.628	<3.88, 95.6	<2.33, 57.3	No stable orbits
HD 96064 Bab	0.217	No stable orbits	No stable orbits	>0.65, 16.1
GJ 896 AB	5.366	<1.79, 11.8	<1.79, 11.8	No stable orbits
GJ 860 AB	2.386	<0.79, 3.17	<0.60, 2.41	>7.15, 28.7
ξ Boo AB	6.345	<2.12, 14.2	<2.12, 14.2	No stable orbits
GJ 166 BC	8.781	<2.20, 10.6	<2.20, 10.6	No stable orbits
GJ 684 AB	1.344	<0.45, 6.34	<0.27, 3.80	>4.03, 56.8
GJ 505 AB	7.512	<2.50, 29.8	<2.50, 29.8	No stable orbits
GJ 702 A	5.160	<1.76, 8.85	<1.32, 6.64	>15.9, 79.7
HD 77407 AB	1.698	<0.57, 17.2	<0.34, 10.23	>5.11, 153.7

Notes. Planets orbiting the primary in a binary star were considered to be de-stabilized by the gravity of the secondary if their apastron distance from the primary was too large. Similarly, planets orbiting the secondary had to have small enough apastron distances to avoid being de-stabilized by the primary. Circumbinary planets had to have a large enough periastron distance to avoid being de-stabilized by the differing gravitation of the two components of the binary. Note that HD 96064B is itself a tight binary star, so planets orbiting it had both a minimum periastron and a maximum apastron.

Table 5
Importance of the M -band Data

Star Name	Total Simulated Detections	Two-band Detections (%)	L' -only Detections (%)	M -only Detections (%)
ϵ Eri	2850	46.98	8.28	44.74
61 Cyg B	1610	52.73	1.55	45.71
61 Cyg A	965	63.01	22.80	14.20
ξ Boo B	157	61.15	18.47	20.38
ξ Boo A	115	60.00	18.26	21.74
GJ 702 A	9	22.22	0.00	77.78

Notes. The usefulness of M -band observations based on our detailed Monte Carlo simulation. When M -band observations were made on a given star, they did substantially increase the number of simulated planets detected around that star.

semimajor axis between 0.3 and 2.5 AU. The mass range for simulated planets was $1\text{--}20 M_{\text{Jup}}$.

We tested three different values of α : -1.1 , -1.31 , and -1.51 , roughly corresponding to the most optimistic permitted, the best-fit, and the most pessimistic permitted values from Cumming et al. (2008). For each value of α , we ran simulations spanning a wide grid in terms of β and R_{trunc} . In contrast to the extensive results described in Section 3.3, the only data saved for these simulations were the probability of finding zero planets. Since we did in fact obtain a null result, distributions for which the probability of this was sufficiently low can be ruled out.

Figures 2 and 3 show the probability of a null result as a function of β and R_{trunc} for our three different values of α . Figure 2 presents constraints based on $\alpha = -1.31$, the best-fit value from RV statistics, while Figure 3 compares the optimistic case $\alpha = -1.1$ and the pessimistic case $\alpha = -1.51$. Each pixel in these figures represents a Monte Carlo simulation involving 15,000 realizations of our survey; generating the figures took several tens of hours on a fast PC. Contours are overlaid at selected probability levels. Regions within the 1%, 5%, and 10% contours can, of course, be ruled out at the 99%, 95%, and 90% confidence levels, respectively. For example, we find that the most optimistic power laws allowed by the Cumming et al. (2008) RV statistics, $\alpha = -1.1$ and $\beta = -0.46$, are ruled out with 90% confidence if R_{trunc} is 110 AU or greater. Similarly,

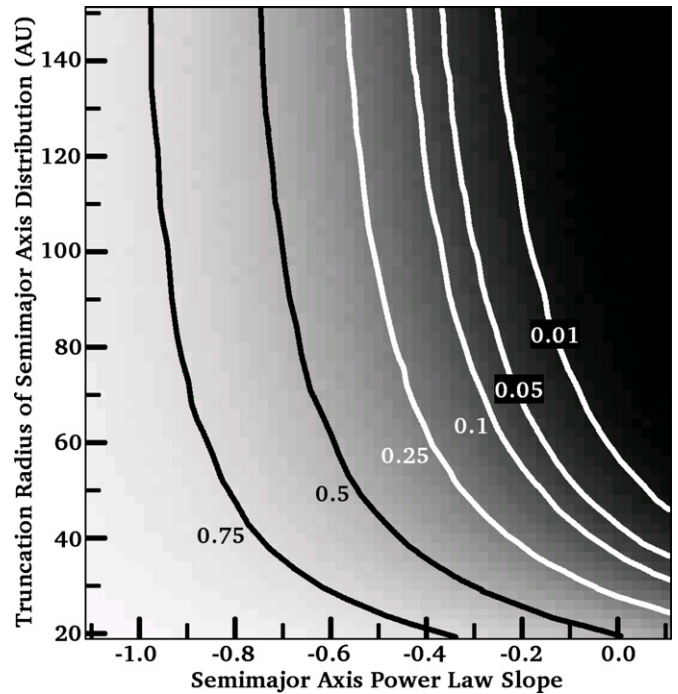


Figure 2. Probability of our survey detecting zero planets, as a function of the power-law slope of the semimajor axis distribution β , where $\frac{dn}{da} \propto a^\beta$, and the outer truncation radius of the semimajor axis distribution. Here, the slope of the mass distribution α has been taken as -1.31 , where $\frac{dn}{dM} \propto M^\alpha$. Since we found no planets, distributions that lead to a probability P of finding no planets are ruled out at the $1 - P$ confidence level: for example, the region above and to the right of the 0.1 contour is ruled out at the 90% confidence level.

$\alpha = -1.51$ and $\beta = -0.3$, truncated at 100 AU, are ruled out. Though $\beta = 0.0$ is not physically plausible, previous work has sometimes used it as an example: for $\alpha = -1.31$, we rule out $\beta = 0.0$ unless R_{trunc} is less than 38 AU.

3.5. Model-independent Constraints

It is also possible to place constraints on the distribution of planets without assuming a power law or any other particular model for the statistics of planetary masses and orbits. Note well that by “model independent” in this context, we mean

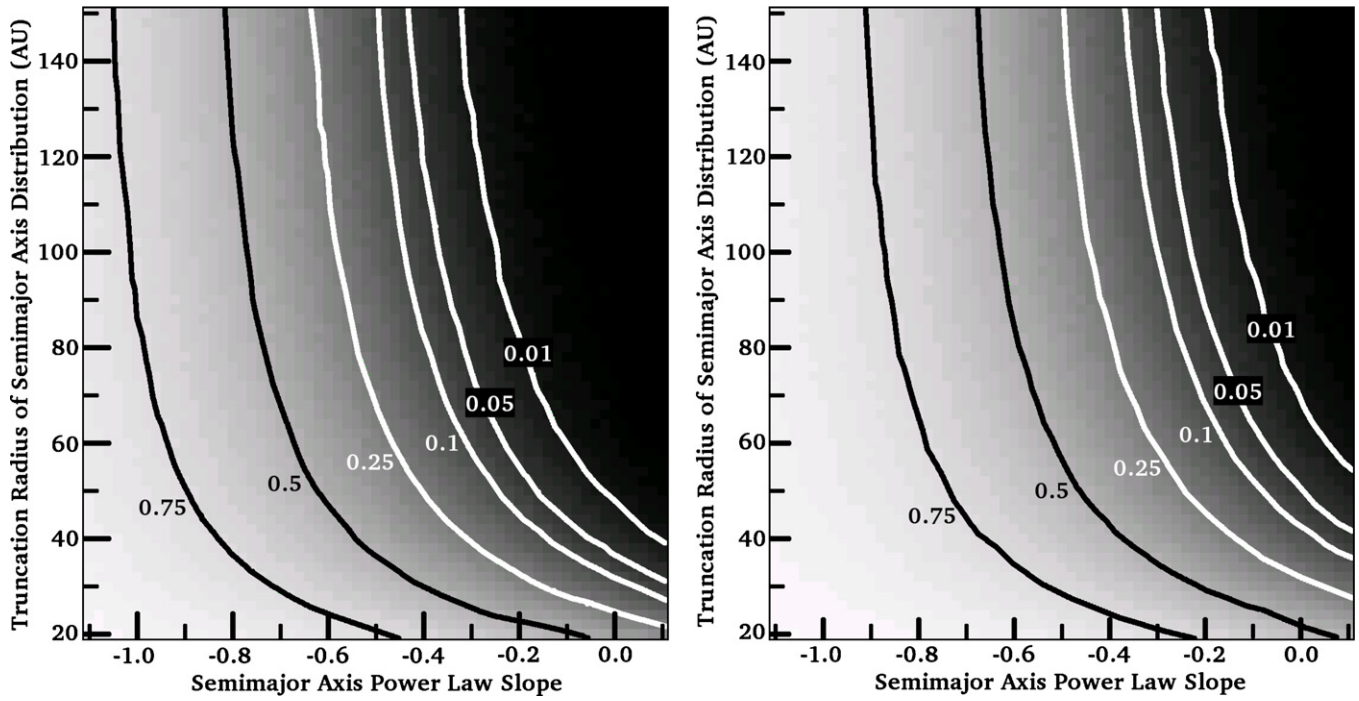


Figure 3. Probability of our survey detecting zero planets, as a function of the power-law slope of the semimajor axis distribution β , where $\frac{dn}{da} \propto a^\beta$, and the outer truncation radius of the semimajor axis distribution. Here, the slope of the mass distribution α has been taken as -1.1 (left) and -1.51 (right), where $\frac{dn}{dM} \propto M^\alpha$. Since we found no planets, distributions that lead to a probability P of finding no planets are ruled out at the $1 - P$ confidence level: for example, the regions above and to the right of the 0.1 contours are ruled out at the 90% confidence level.

independent only of models for the statistical distributions of planets in terms of M and a —not independent of models of planetary *spectra* such as those we obtain from Burrows et al. (2003). The latter are our only means of converting from planetary mass and age to detectable flux, and as such they remain indispensable.

To place our model-independent constraints, we performed an additional series of Monte Carlo simulations on a grid of planet mass and orbital semimajor axis. For each grid point, we seek to determine a number $P(M, a)$ such that, with some specified level of confidence (e.g., 90%), the probability of a star like those in our sample having a planet with the specified mass M and semimajor axis a is no more than $P(M, a)$. We determine $P(M, a)$ by a search: first a guess is made, and a Monte Carlo simulation assuming this probability is performed. If more than 10% of the realizations of our survey turn up a null result, the guessed probability is too low; if less than 10% turn up a null result, the probability is too high. It is adjusted in steps of ever-decreasing size until the correct value is reached.

Figure 4 shows the 90% confidence upper limit on $P(M, a)$ as a function of mass M and semimajor axis a . Each pixel represents thousands of realizations of our survey, with $P(M, a)$ finely adjusted to reach the correct value. Contours are overplotted showing where $P(M, a)$ is less than 8%, 10%, 25%, 50%, and 75%, with 90% confidence. Note that $P(M, a)$, the value constrained by our simulations, is a probability rather than a fixed fraction. The probability is the more scientifically interesting number, but is harder to constrain. For example, if 3.7% is the fraction of the *actual stars in our sample* that have planets with easy-to-detect properties, there are two such planets represented in our 54 star survey. However, if the *probability* of a star like those in our sample having such a planet is 3.7%, there is still a nonzero probability (13% in this case) that no star in our sample actually has such a planet.

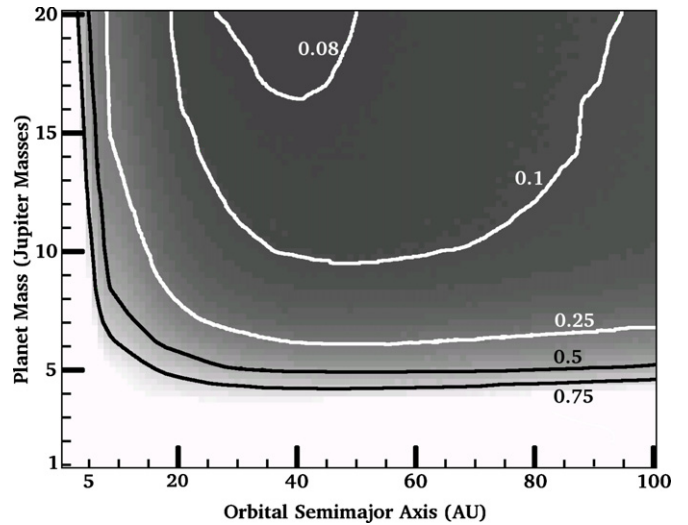


Figure 4. Ninety percent confidence level upper limits on the probability $P(M, a)$ that a star like those in our survey will have a planet of mass M and semimajor axis a . This plot shows, for example, that our survey constrains the abundance of $10 M_{\text{Jup}}$ or more massive planets with orbital semimajor axes between 22 and 100 AU to be less than 15% around Sun-like stars. The abundance of $5 M_{\text{Jup}}$ or more massive planets between 25 and 94 AU is constrained to be less than 50%. The latter range does not extend all the way to 100 AU because our sensitivity to planets in very distant orbits decreases somewhat due to the possibility of their lying beyond our field of view.

The results presented in Figure 4 can be interpreted as model-independent constraints on planet populations. For example, with 90% confidence we find that less than 50% of stars with properties like those in our survey have a $5 M_{\text{Jup}}$ or more massive planet in an orbit with a semimajor axis between 30 and 94 AU. Less than 25% of stars like those in our survey have a $7 M_{\text{Jup}}$ or more massive planet between 25 and 100 AU, less than 15% have

a $10 M_{\text{Jup}}$ or more massive planet between 22 and 100 AU, and less than 12% have a $15 M_{\text{Jup}}$ or more massive planet/brown dwarf between 15 and 100 AU. Going to the most massive objects considered in our simulations, we can set limits ranging inward past 10 AU: we find that less than 25% of stars like those surveyed have a $20 M_{\text{Jup}}$ object orbiting between 8 and 100 AU. These constraints hold independently of how planets are distributed in terms of their masses and semimajor axes.

HR 8799 appears to have a remarkable system of three massive planets, seen at projected distances of 24, 38, and 68 AU, with masses of roughly 10, 10, and $7 M_{\text{Jup}}$, respectively (Marois et al. 2008). Using a Monte Carlo simulation like those used to create Figure 4, we find with 90% confidence that less than 8.1% of stars like those in our survey have a clone of the HR 8799 planetary system. For purposes of this simulation, we adopted the masses above, and set the planets' orbital radii equal to their projected separations. Our 8.1% limit represents a step toward determining whether or not systems of massive planets in wide orbits are more common around more massive stars such as HR 8799 than F, G, K stars such as those we have surveyed.

3.6. Our Survey in the Big Picture

The surveys of Kasper et al. (2007) and Biller et al. (2007) have set constraints on the distributions of extrasolar planets similar to those we present herein, while Nielsen et al. (2008) and especially Lafrenière et al. (2007) have set stronger constraints. More recent analyses by Nielsen & Close (2009) and Chauvin et al. (2010) also provide constraints on the planetary distribution. For example, Nielsen & Close (2009) provide a 68% confidence that the Cumming et al. (2008) distribution can be excluded for a truncation radius of 28 AU. However, if different models are used this number jumps to 83 AU. Chauvin et al. indicate a similar limit from analyzing their results using Baraffe et al. (2003) models. For the standard parameters they indicate a maximum permitted truncation radius of approximately 35 AU. In this context, the results presented here provide looser constraints on the planet distribution, but provide an independent check on the model-dependent systematic errors which may exist with shorter-wavelength data, due to incorrect model brightness estimates or age determination.

Theoretical spectra of self-luminous extrasolar planets are very poorly constrained observationally. The recent detections of possible planets around HR 8799 (Marois et al. 2008), Fomalhaut (Kalas et al. 2008), and β Pic (Lagrange et al. 2009) are either single-band (β Pic) or only beginning to be evaluated at multiple wavelengths (HR 8799, Fomalhaut). The candidate planets orbiting HR 8799 and β Pic are hotter than we would expect to find orbiting middle-aged stars such as those in our survey, while *HST* photometry of Fomalhaut b suggests much of its brightness is starlight reflected from a circumplanetary dust disk. Our survey, and other exoplanet surveys, must therefore be interpreted using models of planetary spectra that are not yet well tested against observations.

Such models predict brightnesses in the *H* band, and particularly in narrow spectral windows within the *H* band that are enormously in excess of blackbody fluxes. The constraints set by Masciadri et al. (2005), Biller et al. (2007), Lafrenière et al. (2007), Nielsen et al. (2008), Nielsen & Close (2009), and Chauvin et al. (2010) depend on the accuracy of these predictions of remarkable brightness in the *H* band. The *L'* and *M* bands that we have used are nearer the blackbody peaks of low-temperature self-luminous planets, and might be expected to be more reliable.

However, Leggett et al. (2007) and Reid & Cruz (2002) suggest that the *M*-band brightness at least of hotter extrasolar planets will be less than that predicted by Burrows et al. (2003) due to above-equilibrium concentrations of CO from convective mixing. Hubeny & Burrows (2007) present new models indicating the effect is present for planets with T_{eff} ranging from 600 to 1800 K. The maximum *M*-band flux suppression is about 40% and flux suppression disappears completely for T_{eff} below 500 K. Based on Burrows et al. (2003), this T_{eff} value corresponds to planets of about 3.5, 6.5, 12, and $15 M_{\text{Jup}}$ at ages of 100 Myr, 300 Myr, 1 Gyr, and 2 Gyr, respectively. In many cases, our *M*-band observations were sensitive to planets at lower masses than these values, and therefore T_{eff} lower than 500 K, implying that the CO flux suppression would have no effect on our mass limits. In other cases, our *M*-band sensitivity did not extend so low. However, given that *M*-band observations formed a relatively small part of our survey, and CO suppression would affect only a fraction even of them, the total effect on the statistical conclusions of our survey should be entirely negligible.

Theoretical spectra such as those of Burrows et al. (2003) may or may not be more reliable in the *L'* and *M* bands than at shorter wavelengths. However, so long as the models remain poorly constrained by observations at every wavelength, conclusions based on observations at multiple wavelengths will be more secure. Our survey, with that of Kasper et al. (2007), has diversified planet imaging surveys across a broader range of wavelengths.

In another sense, our survey differs even from that of Kasper et al. (2007): we have investigated older stars. This is significant because planetary systems up to ages of several hundred Myr may still be undergoing substantial dynamical evolution due to planet–planet interactions (Juric & Tremaine 2008; Gomes et al. 2005). Our survey did not necessarily probe the same planet population as, for example, those of Kasper et al. (2007) and Chauvin et al. (2010).

Finally, theoretical models of older planets are likely more reliable than for younger ones, as these planets are further from their unknown starting conditions and moving toward a well-understood, stable configuration such as that of Jupiter. It has been suggested by Marley et al. (2007) and Fortney et al. (2008) that theoretical planet models such as those of Burrows et al. (2003) and Baraffe et al. (2003) may overpredict the brightness of young (<100 Myr) planets by orders of magnitude, while for older planets the models are more accurate.

We have focused on nearby, mature star systems, and have conservatively handled the ages of stars. This makes our survey uniquely able to confirm that the rarity of giant planets at large separations around solar-type stars, first noticed in surveys strongly weighted toward young stars, persists at older system ages. It is not an artifact of model inaccuracy at young ages due to unknown initial conditions.

4. THE FUTURE OF THE *L'* AND *M* BANDS

In the *L'* and *M* bands, the sky brightness is much worse than at shorter wavelengths. However, models (e.g., Burrows et al. 2003) predict that in the *L'* and *M* bands, planets fade less severely with increasing age (or, equivalently, decreasing T_{eff}). Also, planet/star flux ratios are more favorable in the *L'* and *M* bands than at shorter wavelengths such as the *H* and K_S bands.

It makes sense to use the *L'* and *M* bands on bright stars, where the planet/star flux ratio is a more limiting factor than the sky brightness. In Heinze et al. (2008), we have shown that *M*-band

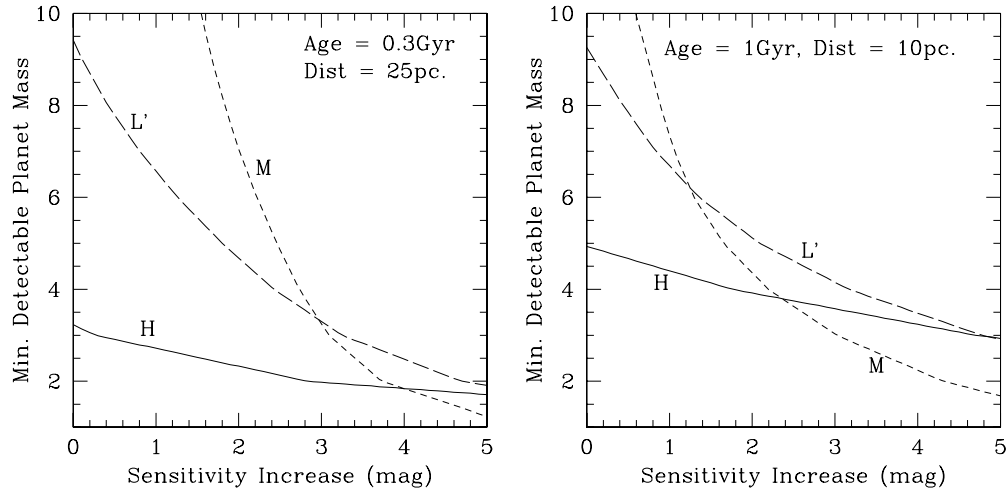


Figure 5. Minimum detectable planet mass in units of M_{Jup} for stars at 25 pc (left) and 10 pc (right), in the H , L' , and M bands, as a function of increase over current sensitivity. We have taken current sensitivities to be $H = 23.0$, $L' = 16.5$, and $M = 13.5$. While the H band will likely remain the wavelength of choice for planet-search observations of stars at 25 pc and beyond, an increase of only 2.4 mag over current sensitivities, even though paralleled by an equal increase in H -band sensitivity, will render the M band more sensitive than H for planets around all stars nearer than 10 pc. The relative effectiveness of different wavelengths depends sensitively on the distance to a star system, but it is essentially independent of the stellar age, as explained in the text.

observations tend to do better than those at shorter wavelengths at small separations from bright stars.

The L' and M bands are most useful, however, for detecting the lowest-temperature planets, which have the reddest $H - L'$ and $H - M$ colors. Such very low temperature planets can only be detected around the nearest stars, so it is for very nearby stars that L' - and M -band observations are most useful. For distant stars, around which only relatively high T_{eff} planets can be detected, the H and K_S bands are much better. We will now quantitatively describe the advantage of L' - and M -band observations over shorter wavelengths for planet-search observations of nearby stars.

Most AO planet searches to date have used the H and K_S bands, or specialized filters in the same wavelength regime. While the K_S band has been used extensively to search for planets around young stars (Masciadri et al. 2005; Chauvin et al. 2010), our comparison here will focus on the H -band regime. Models indicate that it offers better sensitivity than the K_S band except for planets younger than 100 Myr (Burrows et al. 2003; Baraffe et al. 2003), and most of the stars we will suggest the L' and the M bands are useful for will be older than this. The most sensitive H -regime planet-search observations made to date are those of Lafrenière et al. (2007), in part because of their optimized narrowband filter. They attained an effective background-limited point-source sensitivity of about $H = 23.0$. Based on the models of Burrows et al. (2003), Lafrenière et al. (2007) would have set better planetary mass limits than our observations around all of our own survey targets except the very nearest objects, such as ϵ Eri and 61 Cyg. Thus, at present, the H -regime delivers far better planet detection prospects than the L' and M bands for most stars.

However, as detector technology improves, larger telescopes are built, and longer planet detection exposures are attempted, the sensitivity at all wavelengths will increase. This means that low-temperature planets, with their red IR colors, will be detectable at larger distances, and the utility of the L' and especially the M bands will increase. In Figure 5, we show the minimum detectable planet mass for hypothetical stars at 10 and 25 pc distance as a function of the increase over current sensitivity in the H , L' , and M bands, and in Figure 6

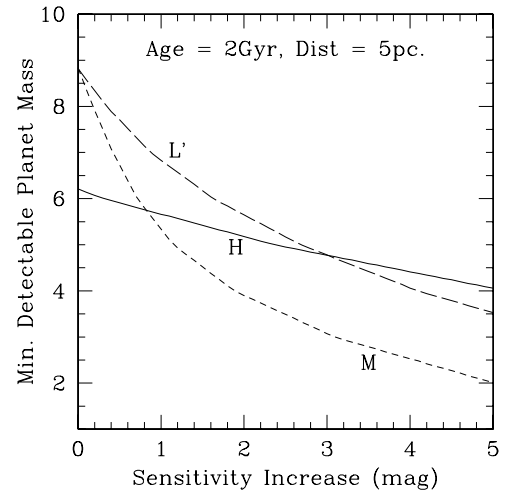


Figure 6. Minimum detectable planet mass in units of M_{Jup} for stars at 5 pc, in the H , L' , and M bands, as a function of increase over current sensitivity. We have taken current sensitivities to be $H = 23.0$, $L' = 16.5$, and $M = 13.5$. Given only a 1 mag increase in M -band sensitivity, paralleled by an equal increase at the H band, the M band would be the best wavelength for planet-search observations around all stars nearer than 5 pc. While the sensitivity increases required to render M preferable in Figure 5 require substantial improvements to existing instruments and telescopes, the 1 mag increase required at 5 pc could be obtained by simply increasing the exposure time. As with Figure 5, this result concerning the relative effectiveness of different wavelengths is independent of stellar age, to first order.

we present the same comparison for a star at 5 pc. We have taken current sensitivity to be $H = 23.0$ (i.e., Lafrenière et al. 2007), $L' = 16.5$, and $M = 13.5$ (i.e., the present work, scaled to an 8 m telescope such as Lafrenière et al. 2007 used). These are background limits, not applicable close to bright stars. Based on Heinze et al. (2008), we believe the L' and M bands will do even better relative to H closer to the star where observations are no longer background limited. Of course, H -band observations with next-generation extreme AO systems such as the Gemini Planet Imager (GPI) and SPHERE will offer improved performance close to the star, but advances in M -band AO coronagraphy (e.g., Kenworthy et al. 2007), will also improve the longer-wavelength results. In any

case, Figures 5 and 6 compare background-limited performance only.

The suppression of flux in the M band due to elevated levels of CO (Leggett et al. 2007; Reid & Cruz 2002) does not apply to planets at the low temperatures relevant for Figures 5 and 6. Based on Burrows et al. (2003), the entire mass range covered by both figures corresponds to planets with T_{eff} below 500 K, except for planets with masses above $6.5 M_{\text{Jup}}$ in the left panel of Figure 5 (25 pc distance, 300 Myr age). This upper section of the 25 pc, 300 Myr panel is irrelevant to the important implications of the figure. According to Hubeny & Burrows (2007), there is no suppression of the M band for effective temperatures below 500 K.

We have deliberately chosen the characteristics of the hypothetical stars in Figures 5 and 6 to be less good than the best available planet-search candidates, so that in each case stars closer and/or younger than the example actually exist. Using the very youngest stars would also have resulted in sensitivities better than $1 M_{\text{Jup}}$, a mass regime not covered by the Burrows et al. (2003) models used in the figures.

Figures 5 and 6 illustrate three very important points. First, the L' band appears to have only secondary usefulness since either the H band or the M band always offers sensitivity to lower-mass planets. Second, Figure 6 shows that with a relatively minor increase of 1 mag in sensitivity, the M band will be sensitive to lower-mass planets around all stars within 5 pc than can be detected with H -band observations, even if the H -band sensitivity increases the same amount. Third, Figure 5 shows that the advantage of the M band decreases with increasing distance, but that as larger telescopes and longer exposures increase sensitivities to 2.5 mag above present levels, the M band will be superior to H out to 10 pc. With an increase of 4 mag, the M band would surpass H out to 25 pc—but as such a large sensitivity increase would be difficult to achieve, the H band will likely remain the primary wavelength for stars at 25 pc and beyond. For stars closer than 10 pc, however, the M band already offers excellent sensitivity that has barely been exploited so far. Given reasonable sensitivity increases, M should become the primary band for planet searches around stars at a distance of 10 pc or less.

Interestingly, the conclusions of Figures 5 and 6 are essentially independent of age: extensive calculations by Heinze (2007) showed that the relative usefulness of different wavelengths had only a weak dependence on age, for stars at a fixed distance—and even this weak age dependence could change sign on switching from the models of Burrows et al. (2003) to those of Baraffe et al. (2003). This means that if we change the ages of the stars in Figures 5 and 6 but leave the distances the same, the L' -, M -, and H -band curves will slide up or down but remain essentially fixed in their relative positions. For example, given a 3 mag increase in sensitivity at both wavelengths, M -band observations will detect lower-mass planets than H -band ones around a star at 10 pc, whether the stellar age is 5 Gyr, 1 Gyr, or 100 Myr. This is to be expected, since if one dials down the age of a given hypothetical star system, the T_{eff} (and therefore IR color) of the faintest detectable planets will remain about the same, though their masses will decrease.

Again, Figures 5 and 6 apply only to background-limited sensitivity. However, given the much more favorable planet/star flux ratios in the M band relative to H , we would expect the longer-wavelength observations to remain equally competitive closer to the star. Advances in M -band coronagraphy will likely parallel the development of H -band extreme AO systems such

as GPI and SPHERE. Though at present they are surpassed in sensitivity by H -regime observations for all but the nearest stars, the L' and especially the M bands hold considerable promise for the future.

5. CONCLUSION

We have surveyed unusually nearby, mature star systems for extrasolar planets in the L' and M bands using the Clio camera with the MMT AO system. By extensive use of blind sensitivity tests involving fake planets inserted into our raw data (reported in detail in Heinze et al. 2010), we established a definitive significance versus completeness relation for planets in our data, which we then used in Monte Carlo simulations to constrain planet distributions.

We set interesting limits on the masses of planets and brown dwarfs in the star systems we surveyed, but we did not detect any planets. Based on this null result, we place constraints on the power laws that may describe the distribution of extrasolar planets in mass and semimajor axis. We also place constraints on planet abundances independent of the distributions. If the distribution of planets is a power law with $dN \propto M^\alpha a^\beta dM da$, the work of Cumming et al. (2008) and Butler et al. (2006) indicates that the most optimistic (i.e., planet-rich) case permitted by the statistics of known RV planets corresponds to about $\alpha = -1.1$ and $\beta = -0.46$. Normalizing the distribution to be consistent with RV statistics, we find that these values of α and β are ruled out at the 90% confidence level, unless the semimajor axis distribution is truncated at a radius R_{trunc} less than 110 AU. Though $\beta = 0.0$ is not physically plausible, previous work has sometimes used it as an example: for $\alpha = -1.31$, corresponding to the best-fit value from Cumming et al. (2008), we rule out $\beta = 0.0$ unless R_{trunc} is less than 38 AU. Independent of distribution models, with 90% confidence no more than 50% of stars like those in our survey have a $5 M_{\text{Jup}}$ or more massive planet orbiting between 30 and 94 AU, no more than 15% have a $10 M_{\text{Jup}}$ planet orbiting between 22 and 100 AU, and no more than 25% have a $20 M_{\text{Jup}}$ object orbiting between 8 and 100 AU.

Our constraints on planet abundances are similar to those placed by Kasper et al. (2007) and Biller et al. (2007), but less tight than those of Nielsen et al. (2008) and especially Lafrenière et al. (2007). The recent work of Nielsen & Close (2009) and Chauvin et al. (2010) also placed tighter constraints on exoplanet distributions than our survey. However, we have surveyed a more nearby, older set of stars than any previous survey, and have therefore placed constraints on a more mature population of planets. Also, we have confirmed that a paucity of giant planets at large separations from Sun-like stars is robustly observed at a wide range of wavelengths.

The best current H -regime observations, those of Lafrenière et al. (2007), would attain sensitivity to lower-mass planets than did our L' - and M -band observations for all of our survey targets except those lying within 4 pc of the Sun. However, as larger telescopes are built and longer exposures are attempted, the sensitivity of M -band observations may be expected to increase at least as fast as that of H -band observations (in part because M -band detectors are currently a less mature technology). As shown in Figures 5 and 6, a modest increase from current sensitivity levels, even if paralleled by an equal increase in H -band sensitivity, would render the M band the wavelength of choice for extrasolar planet searches around a large number of nearby stars.

This research has made use of the SIMBAD online database, operated at CDS, Strasbourg, France, and the VizieR online database (see Ochsenbein et al 2000). We have also made extensive use of information and code from Press et al. (1992). We have used digitized images from the Palomar Sky Survey (available from http://stdatu.stsci.edu/cgi-bin/dss_form), which were produced at the Space Telescope Science Institute under U.S. Government grant NAG W-2166. The images of these surveys are based on photographic data obtained using the Oschin Schmidt Telescope on Palomar Mountain and the UK Schmidt Telescope.

Facilities: MMT, SO:Kuiiper

REFERENCES

- Baraffe, I., Chabrier, G., Barman, T. S., Allard, F., & Hauschildt, P. H. 2003, *A&A*, 402, 701
- Benedict, G., et al. 2006, *AJ*, 132, 2206
- Biller, B. A., et al. 2007, *ApJS*, 173, 143
- Bouchy, F., et al. 2009, *A&A*, 496, 527
- Burrows, A., Sudarsky, D., & Lunine, J. I. 2003, *ApJ*, 596, 578
- Butler, R. P., et al. 2006, *ApJ*, 646, 505
- Charbonneau, D., Brown, T. M., Latham, D. W., & Mayor, M. 2000, *ApJ*, 529, L45
- Chauvin, G., et al. 2010, *A&A*, 509, 52
- Cumming, A., Butler, R. P., Marcy, G. W., Vogt, S. S., Wright, J. T., & Fischer, D. A. 2008, *PASP*, 120, 531
- Fischer, D. A., & Valenti, J. 2005, *ApJ*, 622, 1102
- Fortney, J. J., Marley, M. S., Saumon, D., & Lodders, K. 2008, *ApJ*, 683, 1104
- Gomes, R., Levison, H., Tsiganis, K., & Morbidelli, A. 2005, *Nature*, 435, 466
- Heinze, A. N. 2007, PhD thesis, Univ. Arizona
- Heinze, A. N., Hinz, P. M., Kenworthy, M., Miller, D., & Sivanandam, S. 2008, *ApJ*, 688, 583
- Heinze, A. N., Hinz, P. M., Sivanandam, S., Kenworthy, M., Meyer, M., & Miller, D. 2010, *ApJ*, 714, 1551
- Hubeny, I., & Burrows, A. 2007, *ApJ*, 668, 1248
- Juric, M., & Tremaine, S. 2008, *ApJ*, 686, 603
- Kalas, P., et al. 2008, *Science*, 322, 1345
- Kasper, M., Apai, D., Janson, M., & Brandner, W. 2007, *A&A*, 472, 321
- Kenworthy, M., Codona, J., Johanan, L., Hinz, P., Angel, J., Heinze, A., & Sivanandam, S. 2007, *ApJ*, 660, 762
- Lafrenière, D., et al. 2007, *ApJ*, 670, 1367
- Lagrange, A.-M., et al. 2009, *A&A*, 493, 21
- Leggett, S., Saumon, D., Marley, M., Geballe, T., Golimowski, D., Stephens, D., & Fan, X. 2007, *ApJ*, 655, 1079
- Marley, M. S., Fortney, J. J., Hubickyj, O., Bodenheimer, P., & Lissauer, J. J. 2007, *ApJ*, 655, 541
- Marois, C., Macintosh, B., Barman, T., Zuckerman, B., Song, I., Patience, J., Lafrenière, D., & Doyon, R. 2008, *Science*, 322, 1348
- Masciadri, E., Mundt, R., Henning, Th., Alvarez, C., & Barrado y Navascués, D. 2005, *ApJ*, 625, 1004
- Mayor, M., & Queloz, D. 1995, *Nature*, 378, 355
- Nielsen, E., & Close, L. 2009, arXiv:0909.4531
- Nielsen, E. L., Close, L. M., Biller, B. A., Masciadri, E., & Lenzen, R. 2008, *ApJ*, 674, 466
- Ochsenbein, F., Bauer, P., & Marcout, J. 2000, *A&AS*, 143, 23
- Press, W. H., Teukolsky, S. A., Vetterling, W. T., & Flannery, B. P. 1992, Numerical Recipes in C (2nd ed.; New York, NY: Cambridge Univ. Press)
- Reid, I., & Cruz, K. 2002, *AJ*, 123, 466